Biological Psychiatry: CNNI

Archival Report

Functional and Optogenetic Approaches to Discovering Stable Subtype-Specific Circuit Mechanisms in Depression

Logan Grosenick, Tracey C. Shi, Faith M. Gunning, Marc J. Dubin, Jonathan Downar, and Conor Liston

ABSTRACT

BACKGROUND: Previously, we identified four depression subtypes defined by distinct functional connectivity alterations in depression-related brain networks, which in turn predicted clinical symptoms and treatment response. Optogenetic functional magnetic resonance imaging offers a promising approach for testing how dysfunction in specific circuits gives rise to subtype-specific, depression-related behaviors. However, this approach assumes that there are robust, reproducible correlations between functional connectivity and depressive symptoms—an assumption that was not extensively tested in previous work.

METHODS: First, we comprehensively reevaluated the stability of canonical correlations between functional connectivity and symptoms (N = 220 subjects) using optimized approaches for large-scale statistical hypothesis testing, and we validated methods for improving estimation of latent variables driving brain-behavior correlations. Having confirmed this necessary condition, we reviewed recent advances in optogenetic functional magnetic resonance imaging and illustrated one approach to formulating hypotheses regarding latent subtype-specific circuit mechanisms and testing them in animal models.

RESULTS: Correlations between connectivity features and clinical symptoms were robustly significant, and canonical correlation analysis solutions tested repeatedly on held-out data generalized. However, they were sensitive to data quality, preprocessing, and clinical heterogeneity, which can reduce effect sizes. Generalization could be markedly improved by adding L2 regularization, which decreased estimator variance, increased canonical correlations in left-out data, and stabilized feature selection. These improvements were useful for identifying candidate circuits for optogenetic interrogation in animal models.

CONCLUSIONS: Multiview, latent-variable approaches such as canonical correlation analysis offer a conceptually useful framework for discovering stable patient subtypes by synthesizing multiple clinical and functional measures. Optogenetic functional magnetic resonance imaging holds promise for testing hypotheses regarding latent, subtype-specific mechanisms driving depressive symptoms and behaviors.

Keywords: Biomarkers, Depression, Depression subtypes, Machine learning, Neuroimaging, Optogenetic fMRI

https://doi.org/10.1016/j.bpsc.2019.04.013

Depression is a heterogeneous neuropsychiatric syndrome that is thought to be caused by multiple distinct and interacting neurobiological mechanisms that may play unique roles in various patient subgroups (1–6). Pioneering work identified melancholic, atypical, seasonal, and other clinical subtypes of depression, defined by symptoms or clinical characteristics that tend to co-occur (7–11), but it has been challenging to identify neurobiological correlates that could be used as biomarkers. An alternative strategy for parsing heterogeneity would involve subgrouping patients based on objective biological, cognitive, or behavioral substrates and then testing whether they predict clinical symptoms and outcomes—an approach with proven utility in psychosis, autism, and other disorders (12–17) and, more recently, in depression (18–22).

Our prior work identified four neurophysiological subtypes of depression defined by distinct functional connectivity alterations in limbic and frontostriatal brain networks, which, in turn, predicted distinct clinical symptom profiles (18). We used canonical correlation analysis (CCA) to identify linear combinations of resting-state functional connectivity (RSFC) features that predicted linear combinations of clinical symptoms, both of which could be used for either defining patient subtypes or rating individual patients along continuous dimensions that capture unique aspects of brain dysfunction, consistent with multiple previous studies identifying correlations between RSFC features, symptoms, and diagnostic status (23–32). However, subtype-specific connectivity patterns were complex, and as in other studies (18–21), it remains unclear how

connectivity alterations in specific circuits mediate particular symptoms and behaviors. Addressing this issue will require new approaches aimed at "bridging the causality gap" (33) by experimentally manipulating specific circuits and testing for effects on behavior.

The primary goal of the present work was to illustrate one such approach to formulating hypotheses regarding subtype-specific circuit mechanisms driving depressive behaviors in patients and then testing homologues in animal models using optogenetic functional magnetic resonance imaging (ofMRI). Importantly, this approach assumes that RSFC alterations capture an important latent component of depression pathophysiology that reliably predicts symptoms and behavior. However, a recent preprint study raised questions about this central assumption by showing that CCA involving high-dimensional neuroimaging data tends to overfit and suggesting that RSFC-behavior correlations may not be reliable (34). Thus, a necessary prior goal was to test the assumption that we can reliably reproduce latent variables underlying RSFC-behavior correlations.

We begin by comprehensively reevaluating whether RSFC alterations are stably related to depressive symptoms using optimized approaches for large-scale statistical testing. We find that correlations between RSFC features and clinical symptoms are robustly significant and, further, that latent variable (CCA) solutions tested repeatedly on held-out data generalize, but tend to overfit with increasing numbers of features. To overcome this obstacle, we show that generalization can be markedly improved by adding L2 regularization. Having confirmed these key assumptions, we review recent advances in ofMRI and illustrate how it could be used to causally interrogate latent subtype-specific circuit mechanisms driving particular depression-related behaviors, integrating results from our recent subtyping work with published ofMRI studies. We also discuss pros and cons of this method, relative to lesion analyses and noninvasive brain stimulation methods that can be applied directly in humans.

METHODS AND MATERIALS

Subjects

The analyses reported in Figures 1–3 were designed to reevaluate our approach in our previous work (18) using state-of-the-art statistical methods to test whether depression-related RSFC alterations are significant and stable predictors of clinical symptoms. Therefore, these analyses were conducted in the same subtype-discovery sample used in Drysdale *et al.* (18), which comprised 220 subjects meeting DSM-IV criteria for a diagnosis of (unipolar) major depressive disorder (MDD) and currently experiencing an active, nonpsychotic major depressive episode at the time of the fMRI scan (see Table 1 for details). In addition, to better understand whether differences between this sample (summarized in Supplemental Table S1) and the sample used in Dinga *et al.* (34) may have influenced their power to detect statistically significant RSFC–clinical symptom correlations, we conducted supplementary analyses in a separate sample of 184 subjects (acquired during ongoing studies at Weill Cornell Medicine and Toronto Western Hospital) that more closely resembles their dataset. See Supplemental Methods for further details on subjects and MRI data acquisition.

fMRI Data Preprocessing and RSFC Quantification

Preprocessing was identical to the procedure defined in our previous report (18) and is described in Supplemental Methods.

Data Analysis

The stability and significance of correlations between RSFC features and Hamilton Rating Scale for Depression (HAMD) clinical symptoms was assessed by calculating the 33,123 Pearson correlation coefficients (PCCs) between each RSFC feature and each of 16 of the HAMD item-level measures on 1000 bootstrap replicates to estimate the variance of these correlations (item 17 was excluded, having zero variance in many replicates). We then followed the procedure of Efron (35), using correlation-corrected z values and bootstrapping to calculate the percentage of correlations that exceeded chance level. See Supplemental Methods for further details.

CCA (36,37) was performed between clinical measures and a selected subset of screened RSFC features (those with highest Spearman correlation) as previously described (18). Owing to this feature screening step, we used validation on held-out data in subsequent analyses to avoid overly optimistic correlation estimates due to training-set overfitting. To better stabilize CCA coefficients, L2-regularized CCA (38) was also applied. This approach uses two regularization parameters, λ_X and λ_Y, to regularize the estimated covariance matrices for the RSFC and clinical features, respectively. To find the best combination of these two variables, a grid search over possible values of the parameters and number of features was conducted, with 1000 regularized CCA (RCCA) fits found for each parameter combination. For each set of parameters, model fitting was done on training data and then assessed via the magnitude of the first canonical correlation coefficient on held-out validation test data, using the same procedure as above for standard CCA. See Supplement for further details.

RESULTS

Testing for Robust Correlations Between RSFC Features and Clinical Symptoms

We began with a modern approach to a classical problem: establishing the existence and strength of correlations between brain and behavior using mass univariate statistics. Examining number, strength, and effect size of these correlations gives us a strong basis from which to begin more complicated multivariate analyses (such as CCA) and convinces us of the utility of doing so. Furthermore, understanding the structure of univariate correlations between RSFC and clinical symptoms gives us insight into what kind of challenges might present themselves in the multivariate setting. First, we correlated each RSFC feature with each HAMD clinical symptom and estimated the number of z values for the resulting RSFC-symptom PCCs that exceeded the threshold of significance expected by chance (Figure 1), after correcting for correlations between RSFC features across subjects and for large-scale correlations and multiple comparisons (see

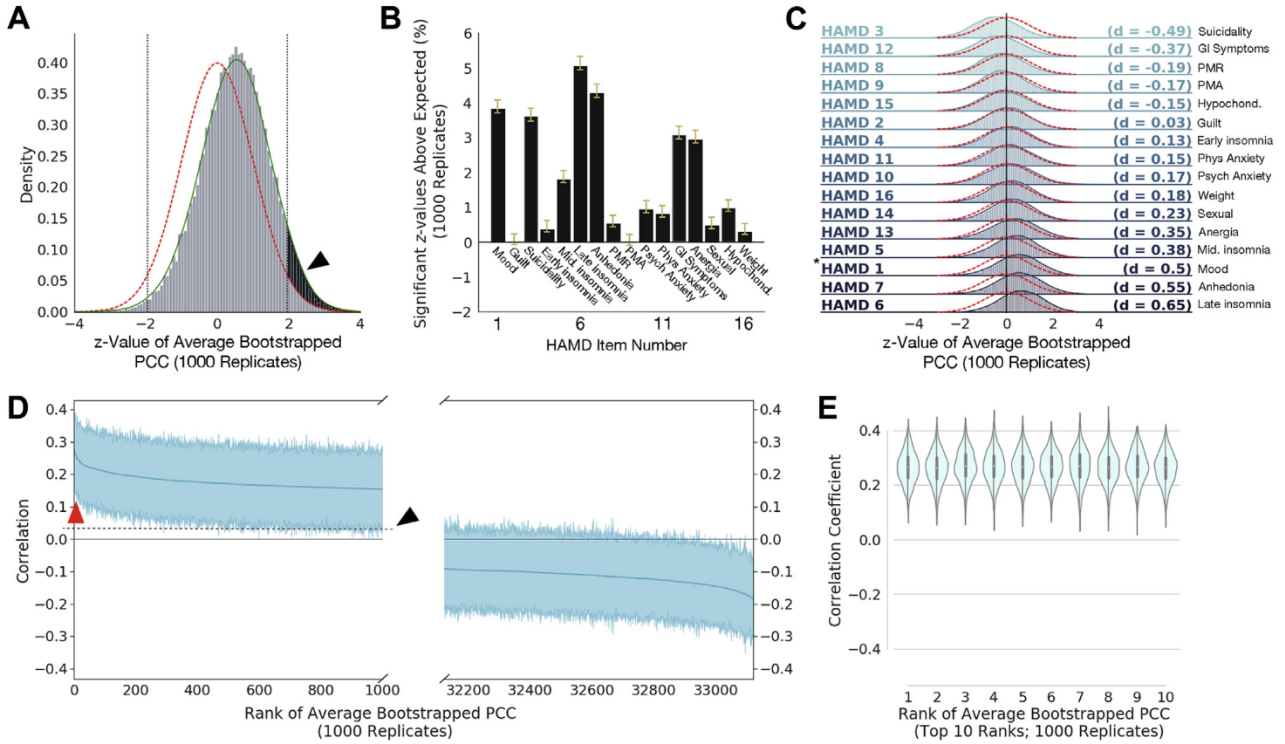

Figure 1. Robust correlations exist between resting-state functional connectivity (RSFC) features and clinical measures (Hamilton Rating Scale for Depression [HAMD]). **(A)** Histogram of z values for the 33,123 average Pearson correlation coefficients (PCCs) between RSFC features and HAMD item 1 (depressed mood) scores averaged over 1000 bootstrap replicates and compared with a standard $\mathcal{N}(0,1)$ Gaussian distribution (red line) and with a smoothed kernel density estimate plotted over the histogram (green line) (see Methods and Materials). The black arrow and shaded region show the area of the z values that exceeds the area expected for a standard normal distribution (outside the two-sided significance criterion of $z > \pm 1.96$ for $p < 0.05$) (shown as vertical dotted black lines). Note the empirical distribution of z values has sample mean and SD $\hat{\mu} = 0.497, \hat{\sigma} = 0.971$, respectively, with the lower-than-expected sample variance resulting from correlations among the statistics; we correct for the effects of such interstatistic correlations using the procedure in Efron (35) (see Methods and Materials). **(B)** Bar plots of the mean percentage of z values that exceeded that expected by chance [e.g., the percentage above 2.5%, shown as the shaded black area in panel **(A)** for HAMD 1] for 1000 bootstrap replicates. Yellow whiskers on the bars denote 95% confidence intervals [corrected for multiple comparisons and data correlation using Bonferroni-Holm and Efron (35), respectively]. HAMD measures 1, 3, 5, 6, 7, 12, and 13 have mean significant percentages well in excess of 1% more than expected under the null hypothesis. **(C)** Histograms of z values similar to histogram shown in panel **(A)** for all 16 HAMD clinical measures considered, ordered by effect size (Cohen's d, given at right of each plot) [magnitudes between 0.2 and 0.5 are considered small to medium effect sizes, and magnitudes between 0.5 and 0.8 are considered medium to large effect sizes; calculated between the smoothed z value distributions similar to the green line in panel **(A)** with the standard normal]. Red dotted lines denote the standard normal distribution. Asterisk marks the distribution for HAMD 1 shown in panel **(A)**. **(D)** Bootstrapped PCCs for HAMD measure 1 for the 1000 most positive (left panel) and 1000 most negative (right panel) RSFC features (shaded regions show 95% percentile bootstrap confidence interval for the mean), ordered by mean correlation (thick blue line). Red arrow points to top 10 most positive-ranked RSFC features [shown in panel **(E)**]; note both have confidence intervals excluding zero, indicating that whereas they cover an appreciable range, they are significantly different than zero across the 1000 bootstrap replicates and thus somewhat stable across bootstrap replicates. The black arrow and dotted line show the upward shift resulting from the positive shift of the distribution shown by the black arrow in panel **(A)**. **(E)** Violin plot (with superimposed boxplots showing first and third quartiles as black bar and the median as white point) of the top 10 positive ranked RSFC features by average PCC to HAMD measure 1 [corresponding to red arrow in panel **(D)**, with mean 95% confidence intervals $\pm$ SD of 0.148 $\pm$ 0.0152, 0.376 $\pm$ 0.0119]. Note these look very similar, suggesting the rank order could easily change across replicates. Symptom abbreviations: Anergia, also encompasses somatic symptoms; Anhedonia, also encompasses work activities; GI, gastrointestinal symptoms; Hypochond., hypochondriasis; Mid., middle insomnia; Phys, physiological anxiety symptoms; PMA, psychomotor agitation; PMR, psychomotor retardation; Psych, psychological anxiety symptoms; Weight, weight loss or weight gain.

Supplemental Methods). We were also interested in establishing the variance of the number of significant correlations: Is it stable, or do small changes in the data collection conditions translate to large changes in the number of correlations that are found to be significant (indicating unstable correlation estimates)?

To estimate the variance of the number of correlations above the significance threshold, we used the bootstrap (39), resampling the RSFC and clinical data for each subject to generate 1000 bootstrap replicate datasets, and then ran the z value procedure from Efron (35) on each. A representative result for HAMD item 1 (HAMD 1: depressed mood) is shown in Figure 1A, with the shaded region showing the number of significant RSFC feature–HAMD 1 correlations above the number expected by chance. We generated confidence intervals for the significant z value estimates with the percentile bootstrap and corrected for the 16 multiple comparisons across the HAMD clinical features using the Holm-Bonferroni procedure, yielding the results shown in Figure 1B, with effect sizes in Figure 1C (40). Seven HAMD measures had median significant percentages (number

Biological Psychiatry: CNNI

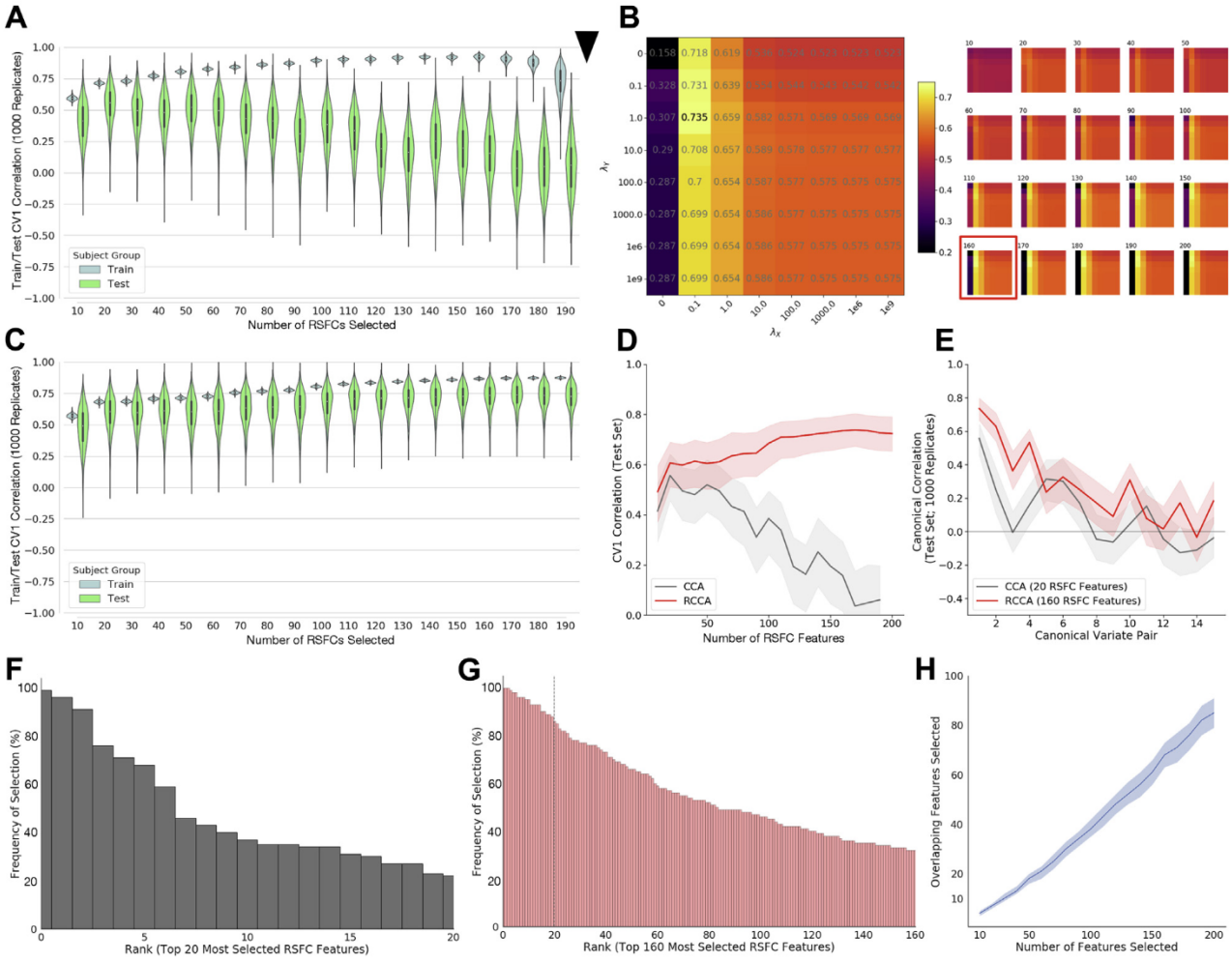

Figure 2. Stable train/test canonical correlations between resting-state functional connectivity (RSFC) features and clinical measures are improved by regularization. **(A)** Violin plots (with superimposed boxplots) of correlations between the first canonical variate (CV1) of a standard canonical correlation analysis (CCA) on training data (90% of subjects) and test data (10% of subjects) for a range of features (10–190 by increments of 10) selected using the correlation method proposed in Drysdale *et al*. (18), with this procedure bootstrapped 1000 times for each number of features to yield the plotted distributions. Feature selection and CCA fitting were done on training data separately for each bootstrap replicate, and then estimated CCA coefficients were applied to the selected features in the held-out validation set to obtain test correlations. Test correlations for CCA peak at 20 features selected. Black arrow shows standard CCA cannot be fit to more correlations than there are observations (in this case 90% of $N = 220$, or 198 subjects). **(B)** Median test rates fit over a grid of regularization parameters λ_X, λ_Y for each number of features selected. (Left panel) The grid corresponding to the best test correlations corresponding to using 160 RSFC features. The color of each square in the grid corresponds to the median test correlation (also printed in gray in the center of each square; color bar at right gives hue values). (Right panel) Similar grids for other numbers of RSFC features (number of features selected shown above grid, test correlations shown in color only, not text). The best fit (160 features; shown on the left) is boxed in red box in the full set of fits on the right. Fitting more than 198 coefficients is possible. **(C)** Violin plots (with superimposed boxplots) of correlations between the first canonical variates of the regularized canonical correlation analysis (RCCA) with the best regularization parameters ($\lambda_X = 0.1$, $\lambda_Y = 1$, $N_F = 160$) on training data (90% of subjects) and test data (10% of subjects) for the various numbers of features selected using the correlation method proposed in Drysdale *et al.* (18) (resampled 1000 times), as in panel **(A)**. Fitting more than 198 coefficients is possible. **(D)** Test rates for CV1 as a function of the number of features selected for CCA (gray) and RCCA (red); shaded region shows first through third quartiles for the replicate fits. **(E)** Test correlations between canonical variates 1–15 for the best fit from panel **(A)** (CCA fit in gray; 20 features) and the best fit from panel **(C)** (RCCA fit in red; 160 features); shaded region shows first through third quartiles for the replicate fits. **(F)** Ordered (by top rank) histogram of the top 20 features chosen by the feature selection approach [from Drysdale *et al.* (18)] showing the percentage of times they were chosen across the 1000 subsampled replicate datasets. Just three features are selected more than 80% of the time. **(G)** Ordered (by top rank) histogram of the top 160 features chosen by the feature selection approach showing the percentage of times they were chosen across 1000 subsampled replicates. Twenty-five features appeared more than 80% of the time (dotted line denotes top 20 features); compare with panel **(F)**. **(H)** Number of overlapping features in all pairwise combinations of 100 randomly chosen replicates as a function of number of features selected (dark blue line shows median, and shaded region shows first through third quartiles across replicates). The median number of overlapping features selected increases approximately linearly with the total number of features selected.

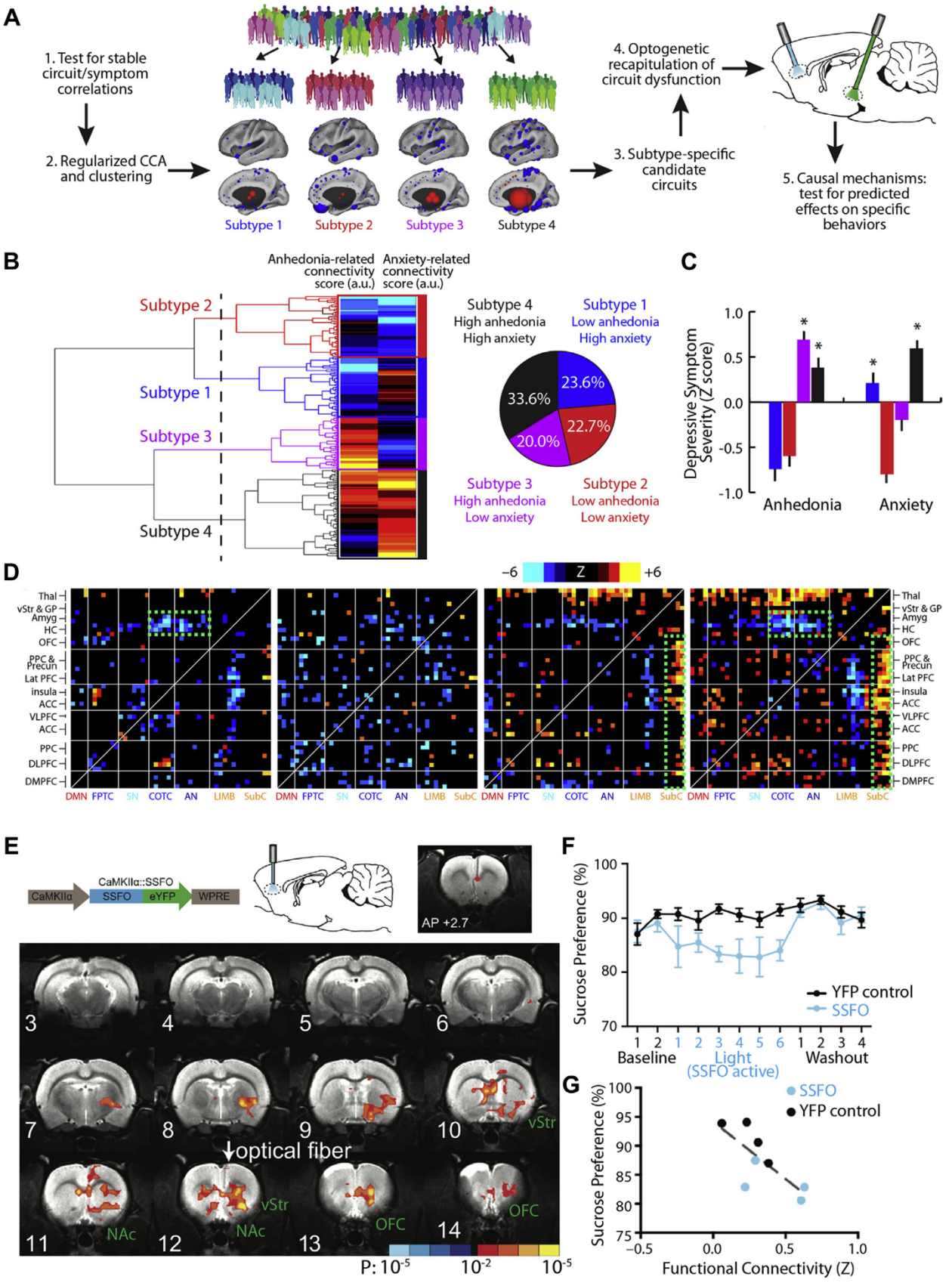
A
1. Test for stable circuit/symptom correlations
2. Regularized CCA and clustering
Subtype 1
Subtype 2
Subtype 3
Subtype 4
3. Subtype-specific candidate circuits
4. Optogenetic recapitulation of circuit dysfunction
5. Causal mechanisms: test for predicted effects on specific behaviors
B
Anhedonia-related connectivity score (a.u.)
Anxiety-related connectivity score (a.u.)
Subtype 2
Subtype 1
Subtype 3
Subtype 4
Subtype 4 High anhedonia High anxiety
Subtype 1 Low anhedonia High anxiety
Subtype 3 High anhedonia Low anxiety
Subtype 2 Low anhedonia Low anxiety
33.6%
23.6%
22.7%
20.0%
C
Depressive Symptom Severity (Z score)
Anhedonia
Anxiety
D
−6 Z +6
Thal
vStr & GP
Amyg
HC
OFC
PPC & Precun
Lat PFC
insula
ACC
VLPFC
ACC
PPC
DLPFC
DMPFC
DMN FPTC SN COTC AN LIMB SubC
E
CaMKIIα::SSFO
CaMKIIα SSFO eYFP WPRE
AP +2.7
3 4 5 6
7 8 9 10
11 12 13 14
vStr
optical fiber
NAc
OFC
P: 10-5 10-2 10-5
F
Sucrose Preference (%)
YFP control
SSFO
Baseline
Light (SSFO active)
Washout
G
SSFO
YFP control
Sucrose Preference (%)
Functional Connectivity (Z)

of correlations more than expected by chance) well in excess of 1% (representing hundreds of significant correlations), and overall, 14 of the 16 *z* value distributions showed reliable, significant shifts in correlations.

We also examined the range of RSFC-HAMD correlations. Figure 1D shows the 1000 most positive (left panel) and 1000 most negative (right panel) correlations, ordered by the average PCC across bootstrap replicates (solid blue line), with 95% confidence intervals (percentile bootstrap). All of the 1000 most positive PCCs and a substantial fraction of the 1000 most negative PCCs had confidence intervals excluding zero, but there was also a significant range over which different bootstrap replicates might yield different orderings of the coefficients. This is illustrated in Figure 1E, showing violin plots detailing the distribution of PCCs for the 10 most positive PCCs: The distributions were significantly different from zero but looked relatively exchangeable, such that their ranking would change over bootstrap replicates. Thus, a large number of very similar variables could result in highly variable feature selection, with implications for CCA discussed below.

RSFC–Clinical Symptom Correlations Are Sensitive to Clinical Sampling and Preprocessing Decisions

Dinga *et al.* in a recent preprint (34) reported the results of an analysis similar to our earlier work (18) and concluded that RSFC–clinical symptom correlations were not significant, which would seem to contradict the findings reported in Figure 1. However, there were several important differences between these two studies (see Supplemental Table S1 for details), especially in their clinical sample characteristics and preprocessing pipelines. Of note, the sample in Dinga *et al.* (34) included 187 subjects scanned on four different scanners (vs. 220 subjects scanned on just two scanners in our previous work, yielding a larger number of subjects per scanner and potentially more stable corrections for scanner-related differences). Among other differences, Dinga *et al.* (34) did

Table 1. Subject Demographics, Medication Status, and Psychiatric Comorbidities

	Toronto Sample	Cornell Sample
Number of Subjects	124	96
Age, Years, Mean	40.4	42.1
Gender, Female, %	57.3	58.3
HAMD-17 Total Score, Mean	20.4	19.3
Psychiatric Medications, %		
Antidepressant	59.7	57.3
Mood stabilizer	16.9	17.7
Antipsychotic	17.7	15.6
Other[a]	45.2	42.7
Psychiatric Comorbidities, %		
Generalized anxiety disorder	4.8	5.2
Posttraumatic stress disorder	6.5	4.2
Social anxiety disorder	4.8	4.2
Panic disorder	2.4	3.1
Other[b]	4.0	3.1

The analyses in Figures 1–3 were implemented in the same dataset used in Drysdale *et al.* (18). Subjects recruited at the Toronto and Cornell sites were matched for age (p = .41), gender (p = .87), and depression severity (HAMD-17 total score, p = .11).

HAMD-17, 17-item Hamilton Rating Scale for Depression.

[a]Psychiatric medications listed as "Other" included benzodiazepines, nonbenzodiazepine sedative-hypnotics, stimulants, and thyroid hormone.

[b]Psychiatric comorbidities listed as "Other" included obsessive-compulsive disorder, attention-deficit/hyperactivity disorder, Asperger's disorder, and Tourette's syndrome.

Figure 3. Optogenetic functional magnetic resonance imaging (fMRI) for interrogating subtype-specific circuit mechanisms in depression. **(A)** Schematic illustration of a model for formulating hypotheses regarding subtype-specific mechanisms driving depressive symptoms and behaviors and testing them in animal models using optogenetic fMRI. By first testing for robust and stable resting-state functional connectivity (RSFC)–clinical symptom correlations as in Figure 1 and then using canonical correlation analysis (CCA) and hierarchical clustering, relatively homogeneous subgroups of a heterogeneous major depressive disorder sample can be identified. These subgroups can be used to identify subtype-specific candidate circuits (see text), and optogenetic fMRI can be used to test hypotheses about dysfunction in specific circuits driving specific behaviors, while also validating whether the RSFC effects evoked by the optogenetic manipulation resemble those observed in human subjects. **(B)** In Drysdale *et al.* (18), hierarchical clustering on two canonical variates representing anhedonia- and anxiety-related RSFC revealed at least four clusters of patients in these two dimensions. The height of each linkage in the dendrogram represents the distance between the clusters joined by that link. The dashed line denotes 20 times the mean distance between pairs of subjects within a cluster. **(C)** The four subtypes predicted significant group differences in anhedonia and anxiety ($p < .005$, Kruskal-Wallis analysis of variance) as indexed by item-level responses on the Hamilton Rating Scale for Depression (items 7 and 11, respectively). Symptom severities are *Z*-scored with respect to the mean and SD of all patients in the sample. Error bars = SEM. **(D)** Heatmaps depicting subtype-specific patterns of altered functional connectivity for the top 50 neuroanatomical regions of interest with the most subtype-specific RSFC features by Kruskal-Wallis analysis of variance. The color scale represents Wilcoxon rank sum test scores for the difference between patients in each subtype and matched healthy control subjects. The green boxes denote RSFC features discussed in the text. For additional details on panels **(B–D)**, see Drysdale *et al.* (18). **(E)** In Ferenczi *et al.* (55), a viral vector (adeno-associated virus/calcium/calmodulin-dependent protein kinase II [CaMKIIa]/stable step function opsin [SSFO]) driving SSFO expression in projection neurons was injected into medial prefrontal cortex (mPFC), and an optical fiber implanted over the mPFC target was used to activate (blue light) and inactivate (amber light) the opsin during alternating resting-state fMRI scanning periods (300 seconds per scan). SSFO activation induced a pattern of increased functional connectivity between an mPFC seed (denoted by the red dot) and a network of structures depicted here, where colors denote the *Z* statistic (and associated *p* value) for RSFC changes in the opsin-on vs. opsin-off conditions (n = 4 rats, 14 runs). **(F)** Subjects (n = 8 SSFO rats, blue; n = 10 control rats, black) were assessed on the sucrose preference test during a 2-day baseline period, followed by 6 days with SSFO activated, followed by a 4-day washout period with SSFO off. SSFO activation reduced sucrose preference behavior ($F_{11,176} = 2.56$, $p = .0051$, two-way repeated measures analysis of variance), compared with subjects expressing a yellow fluorescent protein (YFP) control construct. **(G)** Individual differences in RSFC between the mPFC seed and the ventral striatum correlated with sucrose preference behavior ($R^2 = .56$, $p = .03$). See Drysdale *et al.* (18) and Ferenczi *et al.* (55) for additional details. NAc, nucleus accumbens; OFC, orbitofrontal cortex; vStr, ventral striatum. [Panels **(B–D)** and **(E–G)** modified with permission from Drysdale *et al.* (18) and Ferenczi *et al.* (55), respectively.] ACC, anterior cingulate cortex; AN, attention network; Amyg, amygdala; COTC, cingulo-opercular task-control network; DLPFC, dorsolateral prefrontal cortex; DMN, default mode network; DMPFC, dorsomedial prefrontal cortex; FPTC, frontoparietal task-control network; GP, globus pallidus; HC, hippocampus; LIMB, limbic; OFC, orbitofrontal cortex; PPC, posterior parietal cortex; precun, precuneus; SN, salience network; subC, subcortical; thal, thalamus; VLPFC, ventrolateral prefrontal cortex; VMPFC, ventromedial prefrontal cortex; vStr, ventral striatum.

not directly control for scanner-related differences, and their sample was also more clinically heterogeneous (including MDD, generalized anxiety disorder, social phobia, or panic disorder with no specified requirements for active depressive symptoms vs. currently active, treatment-resistant MDD in our work). By testing for RSFC–clinical symptom correlations in this more heterogeneous sample, the approach in Dinga *et al.* (34) assumes that the mechanisms driving these correlations are the same across these disorders, but this may not be true. For example, it is possible that different mechanisms may drive anxiety symptoms in MDD compared with panic disorder, in which case an analysis of subjects with mixed diagnoses could yield smaller effect sizes and unstable results in held-out data.

To test whether these clinical sample and preprocessing differences could influence their power to detect robust RSFC–clinical symptom correlations, we repeated the analysis reported in Figure 1 in a second, more clinically heterogeneous sample of 184 subjects with MDD or an anxiety disorder, scanned on one of four scanners, and preprocessed exactly as in Dinga *et al.* (34) (see Supplemental Methods). The results in Supplemental Figure S1 show that small but statistically significant RSFC–clinical symptom correlations are still detectable for 10 of 16 symptoms (vs. 14 of 16 in Figure 1B), but these associations are modest, with uniformly small effect sizes (d = 0.21–0.29 for 5 symptoms, $d < 0.2$ for all others). These results are consistent with the interpretation that distinct mechanisms give rise to RSFC–clinical symptom correlations across these heterogeneous disorders and that preprocessing decisions may be important.

Stable Canonical Correlations Between RSFC Features and Clinical Symptoms

CCA (36,37) is a classical multiview statistical approach that we (18) and others (21) have used to find latent linear combinations of RSFC measures and clinical features (canonical variates) that are maximally correlated with each other. In principle, CCA is a potentially useful approach for discovering subtypes of depression (or a dimensional rating system) anchored in brain network dysfunction and for identifying potential latent targets for optogenetic and other causal investigations: It provides a generalizable, low-dimensional representation of the relationship between neuroimaging and clinical features in the form of a simplified summary of the interesting structure between them. However, traditional CCA has some potential weaknesses, particularly on large-scale, correlated data. In particular, CCA coefficients become unstable in the presence of multicollinearity (i.e., significant correlations between variables, as we might suspect between RSFC features and HAMD symptoms) (38). Further, CCA can operate on only as many variables as there are observations, so that feature selection is necessary before applying CCA to reduce the 33,123 RSFC measures to a number less than or equal to the number of subjects in the study (38). Despite this, CCA yielded promising results in recent studies (21) and in the data presented in our previous work (18). However, the stability of CCA solutions was not integral to the other analyses in our previous study (18) and thus was not directly assessed.

To test this, we resampled the data 1000 times (without replacement) into training (90% of subjects) and validation (test) sets (the remaining 10%) and assessed CCA stability by comparing the resulting canonical correlations in the first canonical variate subspace across increasing numbers of RSFC features (Supplemental Methods). Figure 2A shows that standard CCA overfits: The training correlations gradually approached 0.9, whereas the test correlations increased initially but then decreased toward 0.1. The variance of the distributions for test canonical correlations was large, but the best fit had a median canonical correlation of 0.557 (interquartile range = 0.456–0.642), suggesting that the approach is promising.

We hypothesized that these results might be stabilized via L2 regularization applied to the CCA coefficients associated with both the RSFC and the clinical features, as both were multicollinear. L2 regularization [the ridge penalty (41)] induces a small downward bias in coefficient magnitude in exchange for a potentially large reduction in coefficient variance (42). In RCCA, we shrink the sample covariance matrix both for the RSFC features $\widehat{\sum}_X$ and for the clinical measures $\widehat{\sum}_Y$ toward the identity matrix by replacing them with $\widehat{\sum}_X + \lambda_X I$ and $\widehat{\sum}_Y + \lambda_Y I$, respectively (38). This requires specifying the value of the two regularization parameters λ_X and λ_Y for each RCCA fit. To assess the effects of these parameters on fit quality, we fit each of our RCCA models over a grid of λ_X and λ_Y, with each parameter taking values in set $\{0, 0.1, 1, 10, 100, 1000, 1e6, 1e9\}$.

Figure 2B depicts the median canonical correlation results on the held-out test data (over 1000 replicates) and shows that a small amount of regularization of the RSFC feature coefficients greatly improved the test canonical correlations. To a lesser extent, regularization of the HAMD coefficients also benefits fit, with a peak median test canonical correlation at $\lambda_X = 0.1$ and $\lambda_Y = 1.0$ of 0.735 (interquartile range = 0.665–0.797). Compared with the CCA fit in Figure 2A, the test canonical correlations for the best RCCA (fit at $\lambda_X = 0.1$, $\lambda_Y = 1.0$) had lower variance, remained above zero, and improved with increasing number of features (Figure 2C, D). Furthermore, if we examine the stability of test correlations between additional canonical variates (Figure 2E), we see that RCCA uniformly outperforms CCA (at its best performance at 20 RSFC features) for the first four sets of canonical variates. Thus, regularization of both RSFC and HAMD feature coefficients stabilizes and improves low-dimensional coembedding of neuroimaging and clinical measures.

As noted above, Figure 1D showed that a large number of very similar variables could result in highly variable feature selection across bootstrap replicates. Figure 2F and G show the ranked distributions of which RSFC features were chosen by the screening procedure over the 1000 subsamples when selecting the top 20 features (the optimum for traditional CCA in Figure 2A) versus the top 160 features (the optimum for RCCA in Figure 2C). Having just 20 RSFC features (Figure 2F) means just three features are selected more than 80% of the time, whereas having 160 features results in 25 features appearing more than 80% of the time. In Figure 2H, we ran pairwise comparisons looking at how many features appeared in both of two replicates (randomly choosing 100 of the subsample replicates) and found that the number of consistently

selected features increased linearly with the total number of features selected. Thus, stabilizing CCA with regularization allows the model to leverage more features than standard CCA, yielding a broader set of more reliable features that result in higher out-of-sample test correlations.

DISCUSSION

Together, these results support the hypothesis that RSFC alterations capture an important component of the pathophysiology of depression and are robust and reliable predictors of specific symptoms in actively depressed patients with MDD. In particular, as shown in our previous work (18), CCA in this sample revealed two canonical variates, predicting individual differences in 1) anhedonia and psychomotor slowing (HAMD items 7 and 8) and 2) anxiety and insomnia (HAMD items 4, 5, and 11). Individual patients, in turn, could be clustered into subgroups defined by relatively homogeneous patterns of altered functional connectivity in these two dimensions, which predicted distinct clinical symptom and treatment response profiles (Figure 3) (18). Other groups have reported similarly promising results for parsing diagnostic heterogeneity based on task-related and resting-state fMRI (rsfMRI), clinical symptoms, and neuropsychological profiles in affective disorders (19–22) as well as in psychosis and attention-deficit/hyperactivity disorder (12,43–45). For example, Price *et al.* (19) identified two sexually dimorphic subgroups of patients with depression that differed with respect to RSFC in the default mode network and predicted individual differences in comorbid anxiety and history of recurrence. More recently, Xia *et al.* (21) used sparse CCA in a sample of 663 youths with mixed diagnoses to identify four dimensions of altered functional connectivity predicting mood symptoms, psychosis, fear, and externalizing behavior. Importantly, they went on to replicate these findings in an independent sample of 336 subjects, providing further support for the assumption that stable latent-variable relationships between RSFC and clinical symptoms could be used to develop more biologically homogeneous diagnostic labels.

In all of these studies, it remains unclear whether RSFC alterations reflect changes in specific circuits driving depression-related behaviors or are merely correlated with them. Optogenetic tools offer one approach to addressing this question. Over the last 10 years, optogenetic studies have begun to define causal relationships between circuit function and behavior (46–51), with important implications for both neurological (52–54) and psychiatric (49,55–61) diseases. Importantly, these methods can also be integrated with fMRI and other noninvasive neuroimaging techniques that are widely used in humans, offering new opportunities for testing hypotheses and predictions derived from human neuroimaging studies (55,62). Below, we review these developments, illustrate one model for testing such hypotheses, and discuss important caveats and limitations relative to other approaches.

ofMRI for Testing Subtype-Specific Circuit Mechanisms in Depression

First introduced in 2010 (62), ofMRI combines high-field fMRI with photoactivatable opsins to manipulate the activity of genetically defined cellular subtypes and test for local and global effects on neuronal activity and brain network function. The initial report by Lee *et al.* (62) underscored two of the most important and commonly implemented applications of ofMRI. First, it showed how ofMRI could be used to glean mechanistic insights into the neurophysiological basis of the fMRI blood oxygen level–dependent (BOLD) signal—a critical issue for interpreting the results of clinical neuroimaging studies. This report (62) showed that optogenetic stimulation of neocortical or thalamic excitatory neurons was sufficient to drive local BOLD signal responses, informing an ongoing debate about the nature of the neuronal signals and cellular subtypes that underlie the BOLD signal. Subsequent ofMRI studies showed that the BOLD signal is more strongly correlated with local spiking activity than with the local field potential (63) and is driven by the effects of neuronal activity on cerebral venules (64). Recent studies have also shown how inhibitory interneurons and astrocytes contribute to the BOLD signal, independently of activity in excitatory pyramidal neurons and through distinct mechanisms (65,66). Second, Lee *et al.* (62) showed how ofMRI could be used for whole-brain functional circuit mapping, by optogenetically manipulating the activity of excitatory pyramidal cells in a specific brain area and testing for downstream BOLD signal effects. More recent studies extended this approach to map the functional networks activated by specific circuits (e.g., dorsal vs. ventral hippocampus) (67–72) and by specific cellular subtypes (e.g., dopaminergic vs. glutamatergic cells in the ventral tegmental area [VTA]; serotonergic responses to fluoxetine and acute stress) (73–76), often with surprising results that could not be predicted based solely on mapping the axonal projection fields of a given brain region (71,76). Other studies are defining new methods for integrating ofMRI with two-photon microscopy and head-fixed behavior (77,78).

Of particular relevance for translational neuroscience studies, ofMRI methods can also be used to recapitulate disease-related pathophysiological processes and evaluate their impact on brain networks and behavior. To this end, we illustrate one approach for formulating hypotheses regarding subtype-specific mechanisms driving depression-related behaviors and testing them in animal models using ofMRI (Figure 3A), drawing on two recently published works. In this model, rsfMRI is used to identify candidate circuits that predict specific symptoms and behaviors in patients. ofMRI, in turn, can be used to recapitulate and validate these connectivity changes in functionally related circuits in rodents and test for causal effects on associated behaviors. One approach to identifying promising candidate circuits involves searching for connectivity alterations and clinical symptoms that tend to co-occur. For example, in our previous work (18), hierarchical clustering on the two canonical variates described above revealed at least four clusters or subtypes (Figure 3B), predicting group differences in multiple symptoms, especially anhedonia and anxiety (Figure 3C). Group differences in anhedonia and anxiety, in turn, were associated with functional differences in depression-related brain networks (Figure 3D).

These subtype-specific patterns were complex; however, qualitatively, two observations stood out. First, subtypes 1 and 4 were associated with increased anxiety and connectivity deficits in frontoamygdala circuits (Figure 3D: green boxes), which have been implicated in the regulation of fear memories and the cognitive reappraisal of negative emotional states

(79–82). Second, subtypes 3 and 4 were associated with increased anhedonia and hyperconnectivity between the medial prefrontal cortex (mPFC), ventral striatum, and other frontostriatal circuits that have been implicated in reward processing, effort valuation, and motivation (6,27,83–89).

Optogenetic tools provide one means of testing whether altering functional connectivity in these circuits is sufficient for driving specific depression-related behaviors. Stable step function opsins (SSFOs) are particularly useful in this context, in that they were designed to achieve stable, partial depolarization on a timescale of minutes (49), suitable for use in rsfMRI analyses of low-frequency signal fluctuations, but still immediately reversible, enabling within-subject statistical comparisons. Furthermore, by partially depolarizing neurons and rendering them responsive to their physiological inputs, they can, in principle, be used to reversibly modulate functional connectivity in specific circuits and cell types.

A recent ofMRI study by Ferenczi *et al.* (55) provides evidence consistent with the hypothesis that increased functional connectivity in a specific frontostriatal network, qualitatively similar to the pattern observed in subtypes 3 and 4, is sufficient to drive anhedonic behavior in rats. In this study, SSFO was expressed in calcium/calmodulin-dependent protein kinase II alpha-positive projection neurons in the mPFC, and rsfMRI was used to quantify functional connectivity changes elicited by SSFO activation in the mPFC (Figure 3E). SSFO activation increased functional connectivity between the mPFC target and a network of structures, including the ventral striatum, nucleus accumbens, orbitofrontal cortex, anterior cingulate cortex, and thalamus (Figure 3E), qualitatively similar to many of the areas exhibiting increased connectivity in subtypes 3 and 4. SSFO modulation of mPFC projection cells was also sufficient to drive anhedonia-like behavior in the sucrose preference test (Figure 3F, G).

Importantly, this approach also provides a means of testing how circuits interact to produce anhedonic behavior. Ferenczi *et al.* (55) went on to show that mPFC and the VTA compete to influence processing in striatum. VTA stimulation drove a striatal BOLD response that predicted reward-seeking behavior, whereas SSFO modulation of mPFC excitability suppressed the striatal response to VTA stimulation and disrupted reward processing. Of course, these findings do not necessarily indicate that the same mechanism is involved in driving anhedonic behavior in subtypes 3 and 4. Rather, they show that this particular pattern of frontostriatal hyperconnectivity, elicited by increasing the excitability of mPFC projection neurons, is sufficient to disrupt reward-seeking behavior. Future studies could test whether these subtypes are associated with hyperexcitability in mPFC; with deficits in striatal reward reactivity; and with abnormal interactions between VTA, mPFC, and striatum. Likewise, new viral tools for targeting opsin expression to topologically defined projection neuron subtypes with increased ease and efficiency (90–92) will enable more targeted investigations that modulate connectivity between specific nodes in this frontostriatal network.

The example in Figure 3 illustrates one approach to formulating hypotheses about candidate circuits for optogenetic study, based on qualitatively similar connectivity alterations that co-occur with specific symptoms across subtypes. However, candidate circuits could also be identified in a data-driven way, especially with larger sample sizes. Indeed, multiview, latent-variable methods such as RCCA are well suited to this purpose, as reliable latent variables underlying brain-behavior correlations and discovered by RCCA suggest targets for optogenetic interrogation in rodent experiments, which could test whether symptom dimensions can indeed be dissociated by modulating the candidate neural targets. Including sparsity constraints as in the study by Xia *et al.* (21) may further refine candidate targets for optogenetic interrogation using RCCA.

Caveats and Limitations

It is also worth noting some important caveats associated with this approach. First, Figure 2A underscores how CCA has a tendency to overfit when combined with a feature selection step. Therefore, when screening is used to preselect features for further analysis, careful training and test validation are necessary to generate models that perform well in held-out data and to avoid overfitting. Second, the feature selection approach used here is adequate for identifying stable and robust associations between RSFC features and clinical symptoms, but other approaches (e.g., nonlinear multiview and/or sparse methods) could yield superior results.

Third, these approaches may be highly sensitive to clinical sample characteristics (e.g., distinct circuit mechanisms may be at play in active depression, depression in remission, and various anxiety disorders) as well as to medication status, data quality, head motion, and other sources of global signal artifacts. Therefore, it is important to optimize and validate preprocessing methods and other data quality controls based on the goals of a given study. Medication status is an especially important issue: Our sample was treatment resistant, and most subjects were taking at least one psychiatric medication at the time of their scans (Supplemental Table S1). The subtypes did not differ by medication status, indicating that the subtyping results were not likely driven by medication usage per se (18). However, several studies indicate that antidepressants and other psychotropic medications have significant and varied effects on RSFC measures (93–98). Therefore, future studies will be needed to systematically characterize medication effects on resting-state networks and to evaluate the extent to which our results would generalize to unmedicated patients, non–treatment-resistant patients, and first-episode patients.

Fourth, categorical subtyping is just one approach to parsing diagnostic heterogeneity, and the four-cluster solution in Figure 3B is not the only solution. Rather, as discussed in our prior work (18), this four-cluster solution was stable and clinically useful (predicting clinical symptoms and treatment response), but also most likely constrained by features of the subtype discovery dataset, especially sample size and the available clinical data. Item-level HAMD responses provide a relatively coarse, ordinal rating of a limited set of depressive symptoms, and future studies will surely benefit from incorporating more precise rating scales designed to measure specific constructs as well as objective behavioral measures. Likewise, although a model anchored in categorical subtypes provides a familiar and clinically useful heuristic for clinicians to parse diagnostic heterogeneity, other methods might be superior. One alternative approach that warrants further

examination would substitute a multidimensional rating system for categorical subtype diagnoses.

Finally, although we focus here on ofMRI, this approach has some limitations, and other approaches should also be considered. First, it is unclear whether RSFC measures are interpretable in the same way in rodents and primates. A growing body of work highlights qualitative cross-species similarities (99), including a reliable RSFC signal that correlates with low-frequency (delta) power (100,101); robust resting-state functional networks (67,102–105); and a neuroanatomically similar default mode network in both rats and mice (103,106). However, cross-species differences are also evident. For example, the rodent default mode network lacks a neuroanatomical correlate of the primate posterior cingulate areas 23 and 31 (99,106). Likewise, other rsfMRI studies comparing the topology of the mouse, macaque, and human brain have identified reliably conserved properties (e.g., rich club connectivity) but also important differences (e.g., the probability that highly connected hubs are connected to other hubs) (106). Second, some brain circuits in primates may not have clear homologues in rodents. For example, the PFC exhibits a host of cytoarchitectonic, topological, and molecular differences in rodents versus primates (107), and multimodal association cortex occupies a much larger proportion of the human brain (108). Third, rodent models of human behavior are inherently limited to behaviors that are well conserved across species (109), and even superficially similar behaviors and cognitive processes may be implemented by different mechanisms across species (110,111). Consequently, studies drawing parallels between brain circuits and behavior in rodents versus humans must be interpreted with care, and some human brain circuits and behaviors are simply not well modeled in the mouse. In these cases, other approaches, such as concurrent transcranial magnetic stimulation/fMRI (112–114) and new methods for analyzing interactions between brain lesions and their relationship to behavior (115), may be superior for testing causality in the human brain directly (33).

Conclusions

The above caveats notwithstanding, the results in Figures 1–3 and the accompanying review highlight the potential for integrating clinical neuroimaging analyses with ofMRI approaches to formulate and test hypotheses regarding latent, subtype-specific mechanisms underlying depression-related behavior. RCCA can be used to discover robust and stable latent associations between functional connectivity and behavior, linking specific circuits with specific clinical symptom combinations that may be differentially involved in individual patients with MDD. ofMRI, in turn, provides a powerful tool for testing hypotheses derived from clinical neuroimaging data; for implicating specific patterns of network dysfunction as causal mechanisms, not just functional correlates; and for isolating the contributions of specific network nodes and circuits and studying their interactions.

ACKNOWLEDGMENTS AND DISCLOSURES

This work was supported by the National Institute of Mental Health, One Mind Institute, Klingenstein-Simons Foundation Fund, Rita Allen Foundation, Whitehall Foundation, Dana Foundation, Brain and Behavior Research Foundation (National Alliance for Research on Schizophrenia and Depression), Hartwell Foundation, and Simons Foundation Society of Fellows (LG).

We thank Dr. Karl Deisseroth and Dr. Emily Ferenczi for granting permission to adapt selected figure panels from Ferenczi *et al.* (55) for presentation in Figure 3. We also thank Amanda Buch for assistance with illustrating Figure 3.

MJD has received research grants from Neuronetics, Inc., and Tal Medical, Inc. The other authors report no biomedical financial interests or other potential conflicts of interest.

ARTICLE INFORMATION

From the Feil Family Brain and Mind Research Institute and Department of Psychiatry (LG, TCS, FMG, MJD, CL), Weill Cornell Medicine; Department of Statistics (LG), Columbia University; Simons Foundation (LG), New York, New York; and Department of Psychiatry (JD), Toronto Western Hospital, Toronto, Ontario, Canada.

Address correspondence to Conor Liston, M.D., Ph.D., Weill Cornell Medicine, 413 East 69th Street, Box 240, New York, NY 10021; E-mail: col2004@med.cornell.edu.

Received Nov 29, 2018; revised and accepted Apr 29, 2019.

Supplementary material cited in this article is available online at https://doi.org/10.1016/j.bpsc.2019.04.013.

REFERENCES

1. Insel T, Cuthbert B, Garvey M, Heinssen R, Pine DS, Quinn K, *et al.* (2010): Research Domain Criteria (RDoC): Toward a new classification framework for research on mental disorders. Am J Psychiatry 167:748–751.
2. Insel TR, Cuthbert BN (2015): Brain disorders? Precisely. Science 348:499–500.
3. Oathes DJ, Patenaude B, Schatzberg AF, Etkin A (2015): Neurobiological signatures of anxiety and depression in resting-state functional magnetic resonance imaging. Biol Psychiatry 77:385–393.
4. Goodkind M, Eickhoff SB, Oathes DJ, Jiang Y, Chang A, Jones-Hagata LB, *et al.* (2015): Identification of a common neurobiological substrate for mental illness. JAMA Psychiatry 72:305–315.
5. Davidson RJ, Pizzagalli D, Nitschke JB, Putnam K (2002): Depression: Perspectives from affective neuroscience. Annu Rev Psychol 53:545–574.
6. Pizzagalli DA (2014): Depression, stress, and anhedonia: Toward a synthesis and integrated model. Annu Rev Clin Psychol 10:393–423.
7. Wong ML, Kling MA, Munson PJ, Listwak S, Licinio J, Prolo P, *et al.* (2000): Pronounced and sustained central hypernoradrenergic function in major depression with melancholic features: Relation to hypercortisolism and corticotropin-releasing hormone. Proc Natl Acad Sci U S A 97:325–330.
8. Gold PW, Chrousos GP (2002): Organization of the stress system and its dysregulation in melancholic and atypical depression: High vs low CRH/NE states. Mol Psychiatry 7:254–275.
9. Carroll BJ, Feinberg M, Greden JF, Tarika J, Albala AA, Haskett RF, *et al.* (1981): A specific laboratory test for the diagnosis of melancholia—standardization, validation, and clinical utility. Arch Gen Psychiatry 38:15–22.
10. Lewy AJ, Sack RL, Miller LS, Hoban TM (1987): Antidepressant and circadian phase-shifting effects of light. Science 235:352–354.
11. Schatzberg AF, Posener JA, DeBattista C, Kalehzan BM, Rothschild AJ, Shear PK (2000): Neuropsychological deficits in psychotic versus nonpsychotic major depression and no mental illness. Am J Psychiatry 157:1095–1100.
12. Clementz BA, Sweeney JA, Hamm JP, Ivleva EI, Ethridge LE, Pearlson GD, *et al.* (2016): Identification of distinct psychosis biotypes using brain-based biomarkers. Am J Psychiatry 173:373–384.
13. Hill SK, Reilly JL, Keefe RSE, Gold JM, Bishop JR, Gershon ES, *et al.* (2013): Neuropsychological impairments in schizophrenia and psychotic bipolar disorder: Findings from the Bipolar-Schizophrenia Network on Intermediate Phenotypes (B-SNIP) study. Am J Psychiatry 170:1275–1284.

14. Amir RE, Van den Veyver IB, Wan M, Tran CQ, Francke U, Zoghbi HY (1999): Rett syndrome is caused by mutations in X-linked MECP2, encoding methyl-CpG-binding protein 2. Nat Genet 23:185–188.
15. Baron-Cohen S, Wheelwright S (2004): The empathy quotient: An investigation of adults with Asperger syndrome or high functioning autism, and normal sex differences. J Autism Dev Disord 34:163–175.
16. Sebat J, Lakshmi B, Malhotra D, Troge J, Lese-Martin C, Walsh T, *et al.* (2007): Strong association of de novo copy number mutations with autism. Science 316:445–449.
17. Pinto D, Pagnamenta AT, Klei L, Anney R, Merico D, Regan R, *et al.* (2010): Functional impact of global rare copy number variation in autism spectrum disorders. Nature 466:368–372.
18. Drysdale AT, Grosenick L, Downar J, Dunlop K, Mansouri F, Meng Y, *et al.* (2017): Resting-state connectivity biomarkers define neurophysiological subtypes of depression. Nat Med 23:28–38.
19. Price RB, Gates K, Kraynak TE, Thase ME, Siegle GJ (2017): Data-driven subgroups in depression derived from directed functional connectivity paths at rest. Neuropsychopharmacology 42:2623–2632.
20. Price RB, Lane S, Gates K, Kraynak TE, Horner MS, Thase ME, Siegle GJ (2017): Parsing heterogeneity in the brain connectivity of depressed and healthy adults during positive mood. Biol Psychiatry 81:347–357.
21. Xia CH, Ma Z, Ciric R, Gu S, Betzel RF, Kaczkurkin AN, *et al.* (2018): Linked dimensions of psychopathology and connectivity in functional brain networks. Nat Commun 9:3003.
22. Grisanzio KA, Goldstein-Piekarski AN, Wang MY, Rashed Ahmed AP, Samara Z, Williams LM (2018): Transdiagnostic symptom clusters and associations with brain, behavior, and daily function in mood, anxiety, and trauma disorders. JAMA Psychiatry 75:201–209.
23. Greicius MD, Flores BH, Menon V, Glover GH, Solvason HB, Kenna H, *et al.* (2007): Resting-state functional connectivity in major depression: Abnormally increased contributions from subgenual cingulate cortex and thalamus. Biol Psychiatry 62:429–437.
24. Pezawas L, Meyer-Lindenberg A, Drabant EM, Verchinski BA, Munoz KE, Kolachana BS, *et al.* (2005): 5-HTTLPR polymorphism impacts human cingulate-amygdala interactions: A genetic susceptibility mechanism for depression. Nat Neurosci 8:828–834.
25. Sheline YI, Price JL, Yan Z, Mintun MA (2010): Resting-state functional MRI in depression unmasks increased connectivity between networks via the dorsal nexus. Proc Natl Acad Sci U S A 107:11020–11025.
26. Sheline YI, Barch DM, Price JL, Rundle MM, Vaishnavi SN, Snyder AZ, *et al.* (2009): The default mode network and self-referential processes in depression. Proc Natl Acad Sci U S A 106:1942–1947.
27. Knutson B, Bhanji JP, Cooney RE, Atlas LY, Gotlib IH (2008): Neural responses to monetary incentives in major depression. Biol Psychiatry 63:686–692.
28. Liston C, Chen AC, Zebley BD, Drysdale AT, Gordon R, Leuchter B, *et al.* (2014): Default mode network mechanisms of transcranial magnetic stimulation in depression. Biol Psychiatry 76:517–526.
29. Broyd SJ, Demanuele C, Debener S, Helps SK, James CJ, Sonuga-Barke EJS (2009): Default-mode brain dysfunction in mental disorders: A systematic review. Neurosci Biobehav Rev 33:279–296.
30. Anand A, Li Y, Wang Y, Wu J, Gao S, Bukhari L, *et al.* (2005): Activity and connectivity of brain mood regulating circuit in depression: A functional magnetic resonance study. Biol Psychiatry 57:1079–1088.
31. Kaiser RH, Andrews-Hanna JR, Wager TD, Pizzagalli DA (2015): Large-scale network dysfunction in major depressive disorder: A meta-analysis of resting-state functional connectivity. JAMA Psychiatry 72:603–611.
32. McTeague LM, Huemer J, Carreon DM, Jiang Y, Eickhoff SB, Etkin A (2017): Identification of common neural circuit disruptions in cognitive control across psychiatric disorders. Am J Psychiatry 174:676–685.
33. Etkin A (2018): Addressing the causality gap in human psychiatric neuroscience. JAMA Psychiatry 75:3–4.
34. Dinga R, Schmaal L, Penninx BWJH, van Tol MJ, Veltman DJ, van Velzen L, *et al.* (2019): Evaluating the evidence for biotypes of depression: Methodological replication and extension of Drysdale et al. (2017) [published online ahead of print Mar 27]. Neuroimage Clin.
35. Efron B (2010): Correlated z-values and the accuracy of large-scale statistical estimates. J Am Stat Assoc 105:1042–1055.
36. Hotelling H (1936): Relations between two sets of variates. Biometrika 28:321–377.
37. Hardoon DR, Szedmak S, Shawe-Taylor J (2004): Canonical correlation analysis: An overview with application to learning methods. Neural Comput 16:2639–2664.
38. Gonzalez I, Dejean S, Martin PGP, Baccini A (2008): CCA: An R Package to Extend Canonical Correlation Analysis. Journal of Statistical Software 23(12). Available at https://core.ac.uk/download/pdf/6303071.pdf. Accessed May 1, 2019.
39. Efron B, Tibshirani RJ (1994): An Introduction to the Bootstrap. Boca Raton, FL: CRC Press.
40. Cohen J (1988): Statistical Power Analysis for the Behavioral Sciences, 2nd ed. Hillsdale, NJ: Lawrence Erlbaum.
41. Hoerl AE, Kennard RW (1970): Ridge regression: Biased estimation for nonorthogonal problems. Technometrics 12:55–67.
42. Hastie T, Tibshirani R, Friedman J (2009): The Elements of Statistical Learning: Data Mining, Inference, and Prediction, 2nd ed. Springer Series in Statistics. New York: Springer.
43. Karalunas SL, Fair D, Musser ED, Aykes K, Iyer SP, Nigg JT (2014): Subtyping attention-deficit/hyperactivity disorder using temperament dimensions: Toward biologically based nosologic criteria. JAMA Psychiatry 71:1015–1024.
44. Cao H, Chén OY, Chung Y, Forsyth JK, McEwen SC, Gee DG, *et al.* (2018): Cerebello-thalamo-cortical hyperconnectivity as a state-independent functional neural signature for psychosis prediction and characterization. Nat Commun 9:3836.
45. Yang Z, Xu Y, Xu T, Hoy CW, Handwerker DA, Chen G, *et al.* (2014): Brain network informed subject community detection in early-onset schizophrenia. Sci Rep 4:5549.
46. Boyden ES, Zhang F, Bamberg E, Nagel G, Deisseroth K (2005): Millisecond-timescale, genetically targeted optical control of neural activity. Nat Neurosci 8:1263–1268.
47. Cardin JA, Carlén M, Meletis K, Knoblich U, Zhang F, Deisseroth K, *et al.* (2009): Driving fast-spiking cells induces gamma rhythm and controls sensory responses. Nature 459:663–667.
48. Zhang F, Wang LP, Brauner M, Liewald JF, Kay K, Watzke N, *et al.* (2007): Multimodal fast optical interrogation of neural circuitry. Nature 446:633–639.
49. Yizhar O, Fenno LE, Prigge M, Schneider F, Davidson TJ, O'Shea DJ, *et al.* (2011): Neocortical excitation/inhibition balance in information processing and social dysfunction. Nature 477:171–178.
50. Chow BY, Han X, Dobry AS, Qian X, Chuong AS, Li M, *et al.* (2010): High-performance genetically targetable optical neural silencing by light-driven proton pumps. Nature 463:98–102.
51. Grosenick L, Marshel JH, Deisseroth K (2015): Closed-loop and activity-guided optogenetic control. Neuron 86:106–139.
52. Adamantidis AR, Zhang F, Aravanis AM, Deisseroth K, de Lecea L (2007): Neural substrates of awakening probed with optogenetic control of hypocretin neurons. Nature 450:420–424.
53. Gradinaru V, Mogri M, Thompson KR, Henderson JM, Deisseroth K (2009): Optical deconstruction of parkinsonian neural circuitry. Science 324:354–359.
54. Kravitz AV, Freeze BS, Parker PRL, Kay K, Thwin MT, Deisseroth K, Kreitzer AC (2010): Regulation of parkinsonian motor behaviours by optogenetic control of basal ganglia circuitry. Nature 466:622–626.
55. Ferenczi EA, Zalocusky KA, Liston C, Grosenick L, Warden MR, Amatya D, *et al.* (2016): Prefrontal cortical regulation of brainwide circuit dynamics and reward-related behavior. Science 351:aac9698.
56. Covington HE, Lobo MK, Maze I, Vialou V, Hyman JM, Zaman S, *et al.* (2010): Antidepressant effect of optogenetic stimulation of the medial prefrontal cortex. J Neurosci 30:16082–16090.
57. Chaudhury D, Walsh JJ, Friedman AK, Juarez B, Ku SM, Koo JW, *et al.* (2013): Rapid regulation of depression-related behaviours by control of midbrain dopamine neurons. Nature 493:532–536.

58. Tye KM, Prakash R, Kim SY, Fenno LE, Grosenick L, Zarabi H, *et al.* (2011): Amygdala circuitry mediating reversible and bidirectional control of anxiety. Nature 471:358–362.
59. Lammel S, Lim BK, Ran C, Huang KW, Betley MJ, Tye KM, *et al.* (2012): Input-specific control of reward and aversion in the ventral tegmental area. Nature 491:212–217.
60. Stuber GD, Sparta DR, Stamatakis AM, van Leeuwen WA, Hardjoprajitno JE, Cho S, *et al.* (2011): Excitatory transmission from the amygdala to nucleus accumbens facilitates reward seeking. Nature 475:377–380.
61. Ciocchi S, Herry C, Grenier F, Wolff SBE, Letzkus JJ, Vlachos I, *et al.* (2010): Encoding of conditioned fear in central amygdala inhibitory circuits. Nature 468:277–282.
62. Lee JH, Durand R, Gradinaru V, Zhang F, Goshen I, Kim DS, *et al.* (2010): Global and local fMRI signals driven by neurons defined optogenetically by type and wiring. Nature 465:788–792.
63. Kahn I, Knoblich U, Desai M, Bernstein J, Graybiel AM, Boyden ES, *et al.* (2013): Optogenetic drive of neocortical pyramidal neurons generates fMRI signals that are correlated with spiking activity. Brain Res 1511:33–45.
64. Yu X, He Y, Wang M, Merkle H, Dodd SJ, Silva AC, Koretsky AP (2016): Sensory and optogenetically driven single-vessel fMRI. Nat Methods 13:337–340.
65. Vazquez AL, Fukuda M, Kim SG (2018): Inhibitory neuron activity contributions to hemodynamic responses and metabolic load examined using an inhibitory optogenetic mouse model. Cereb Cortex 28:4105–4119.
66. Takata N, Sugiura Y, Yoshida K, Koizumi M, Hiroshi N, Honda K, *et al.* (2018): Optogenetic astrocyte activation evokes BOLD fMRI response with oxygen consumption without neuronal activity modulation. Glia 66:2013–2023.
67. Liang Z, Watson GDR, Alloway KD, Lee G, Neuberger T, Zhang N (2015): Mapping the functional network of medial prefrontal cortex by combining optogenetics and fMRI in awake rats. Neuroimage 117:114–123.
68. Chan RW, Leong ATL, Ho LC, Gao PP, Wong EC, Dong CM, *et al.* (2017): Low-frequency hippocampal-cortical activity drives brain-wide resting-state functional MRI connectivity. Proc Natl Acad Sci U S A 114:E6972–E6981.
69. Leong ATL, Chan RW, Gao PP, Chan YS, Tsia KK, Yung WH, Wu EX (2016): Long-range projections coordinate distributed brain-wide neural activity with a specific spatiotemporal profile. Proc Natl Acad Sci U S A 113:E8306–E8315.
70. Weitz AJ, Fang Z, Lee HJ, Fisher RS, Smith WC, Choy M, *et al.* (2015): Optogenetic fMRI reveals distinct, frequency-dependent networks recruited by dorsal and intermediate hippocampus stimulations. Neuroimage 107:229–241.
71. Takata N, Yoshida K, Komaki Y, Xu M, Sakai Y, Hikishima K, *et al.* (2015): Optogenetic activation of CA1 pyramidal neurons at the dorsal and ventral hippocampus evokes distinct brain-wide responses revealed by mouse fMRI. PLoS One 10:e0121417.
72. Benekareddy M, Stachniak TJ, Bruns A, Knoflach F, von Kienlin M, Künnecke B, Ghosh A (2018): Identification of a corticohabenular circuit regulating socially directed behavior. Biol Psychiatry 83:607–617.
73. Bernal-Casas D, Lee HJ, Weitz AJ, Lee JH (2017): Studying brain circuit function with dynamic causal modeling for optogenetic fMRI. Neuron 93:522–532.e5.
74. Lee HJ, Weitz AJ, Bernal-Casas D, Duffy BA, Choy M, Kravitz AV, *et al.* (2016): Activation of direct and indirect pathway medium spiny neurons drives distinct brain-wide responses. Neuron 91:412–424.
75. Brocka M, Helbing C, Vincenz D, Scherf T, Montag D, Goldschmidt J, *et al.* (2018): Contributions of dopaminergic and non-dopaminergic neurons to VTA-stimulation induced neurovascular responses in brain reward circuits. Neuroimage 177:88–97.
76. Grandjean J, Corcoba A, Kahn MC, Upton AL, Deneris ES, Seifritz E, *et al.* (2019): A brain-wide functional map of the serotonergic responses to acute stress and fluoxetine. Nat Commun 10:350.
77. Han Z, Chen W, Chen X, Zhang K, Tong C, Zhang X, *et al.* (2019): Awake and behaving mouse fMRI during Go/No-Go task. Neuroimage 188:733–742.
78. Desjardins M, Kılıç K, Thunemann M, Mateo C, Holland D, Ferri CGL, *et al.* (2019): Awake mouse imaging: From two-photon microscopy to blood oxygen–level dependent functional magnetic resonance imaging. Biol Psychiatry Cogn Neurosci Neuroimaging 4:533–542.
79. Wager TD, Davidson ML, Hughes BL, Lindquist MA, Ochsner KN (2008): Prefrontal-subcortical pathways mediating successful emotion regulation. Neuron 59:1037–1050.
80. Milad MR, Quirk GJ (2002): Neurons in medial prefrontal cortex signal memory for fear extinction. Nature 420:70–74.
81. Phelps EA, Delgado MR, Nearing KI, LeDoux JE (2004): Extinction learning in humans: Role of the amygdala and vmPFC. Neuron 43:897–905.
82. Ochsner KN, Gross JJ (2005): The cognitive control of emotion. Trends Cogn Sci 9:242–249.
83. Pizzagalli DA, Holmes AJ, Dillon DG, Goetz EL, Birk JL, Bogdan R, *et al.* (2009): Reduced caudate and nucleus accumbens response to rewards in unmedicated individuals with major depressive disorder. Am J Psychiatry 166:702–710.
84. Kvitsiani D, Ranade S, Hangya B, Taniguchi H, Huang JZ, Kepecs A (2013): Distinct behavioural and network correlates of two interneuron types in prefrontal cortex. Nature 498:363–366.
85. Hillman KL, Bilkey DK (2012): Neural encoding of competitive effort in the anterior cingulate cortex. Nat Neurosci 15:1290–1297.
86. Croxson PL, Walton ME, O'Reilly JX, Behrens TEJ, Rushworth MFS (2009): Effort-based cost-benefit valuation and the human brain. J Neurosci 29:4531–4541.
87. Treadway MT, Bossaller NA, Shelton RC, Zald DH (2012): Effort-based decision-making in major depressive disorder: A translational model of motivational anhedonia. J Abnorm Psychol 121:553–558.
88. Schultz W, Dayan P, Montague PR (1997): A neural substrate of prediction and reward. Science 275:1593–1599.
89. Cardinal RN, Parkinson JA, Hall J, Everitt BJ (2002): Emotion and motivation: The role of the amygdala, ventral striatum, and prefrontal cortex. Neurosci Biobehav Rev 26:321–352.
90. Tervo DG, Hwang BY, Viswanathan S, Gaj T, Lavzin M, Ritola KD, *et al.* (2016): A designer AAV variant permits efficient retrograde access to projection neurons. Neuron 92:372–382.
91. Luo L, Callaway EM, Svoboda K (2018): Genetic dissection of neural circuits: A decade of progress. Neuron 98:256–281.
92. Beier KT, Steinberg EE, DeLoach KE, Xie S, Miyamichi K, Schwarz L, *et al.* (2015): Circuit architecture of VTA dopamine neurons revealed by systematic input-output mapping. Cell 162:622–634.
93. Anand A, Li Y, Wang Y, Gardner K, Lowe MJ (2007): Reciprocal effects of antidepressant treatment on activity and connectivity of the mood regulating circuit: An fMRI study. J Neuropsychiatry Clin Neurosci 19:274–282.
94. Anand A, Li Y, Wang Y, Wu JW, Gao SJ, Bukhari L, *et al.* (2005): Antidepressant effect on connectivity of the mood-regulating circuit: An fMRI study. Neuropsychopharmacology 30:1334–1344.
95. Scheidegger M, Walter M, Lehmann M, Metzger C, Grimm S, Boeker H, *et al.* (2012): Ketamine decreases resting state functional network connectivity in healthy subjects: Implications for antidepressant drug action. PLoS One 7:e44799.
96. McCabe C, Mishor Z (2011): Antidepressant medications reduce subcortical-cortical resting-state functional connectivity in healthy volunteers. Neuroimage 57:1317–1323.
97. Posner J, Hellerstein DJ, Gat I, Mechling A, Klahr K, Wang Z, *et al.* (2013): Antidepressants normalize the default mode network in patients with dysthymia. JAMA Psychiatry 70:373–382.
98. Wang L, Xia M, Li K, Zeng Y, Su Y, Dai W, *et al.* (2015): The effects of antidepressant treatment on resting-state functional brain networks in patients with major depressive disorder. Hum Brain Mapp 36:768–778.
99. Gozzi A, Schwarz AJ (2016): Large-scale functional connectivity networks in the rodent brain. Neuroimage 127:496–509.
100. Lu H, Zuo Y, Gu H, Waltz JA, Zhan W, Scholl CA, *et al.* (2007): Synchronized delta oscillations correlate with the resting-state functional MRI signal. Proc Natl Acad Sci U S A 104:18265–18269.

101. Zuo XN, Di Martino A, Kelly C, Shehzad ZE, Gee DG, Klein DF, *et al.* (2010): The oscillating brain: Complex and reliable. Neuroimage 49:1432–1445.
102. Hutchison RM, Mirsattari SM, Jones CK, Gati JS, Leung LS (2010): Functional networks in the anesthetized rat brain revealed by independent component analysis of resting-state FMRI. J Neurophysiol 103:3398–3406.
103. Lu H, Zou Q, Gu H, Raichle ME, Stein EA, Yang Y (2012): Rat brains also have a default mode network. Proc Natl Acad Sci U S A 109:3979–3984.
104. Liang Z, King J, Zhang N (2012): Anticorrelated resting-state functional connectivity in awake rat brain. Neuroimage 59:1190–1199.
105. Grandjean J, Schroeter A, Batata I, Rudin M (2014): Optimization of anesthesia protocol for resting-state fMRI in mice based on differential effects of anesthetics on functional connectivity patterns. Neuroimage 102(Pt 2):838–847.
106. Stafford JM, Jarrett BR, Miranda-Dominguez O, Mills BD, Cain N, Mihalas S, *et al.* (2014): Large-scale topology and the default mode network in the mouse connectome. Proc Natl Acad Sci U S A 111:18745–18750.
107. Ongur D, Price JL (2000): The organization of networks within the orbital and medial prefrontal cortex of rats, monkeys and humans. Cereb Cortex 10:206–219.
108. Buckner RL, Krienen FM (2013): The evolution of distributed association networks in the human brain. Trends Cogn Sci 17:648–665.
109. Nestler EJ, Hyman SE (2010): Animal models of neuropsychiatric disorders. Nat Neurosci 13:1161–1169.
110. Redish AD (2004): Addiction as a computational process gone awry. Science 306:1944–1947.
111. Sweis BM, Abram SV, Schmidt BJ, Seeland KD, MacDonald AW, Thomas MJ, Redish AD (2018): Sensitivity to "sunk costs" in mice, rats, and humans. Science 361:178–181.
112. Ruff CC, Blankenburg F, Bjoertomt O, Bestmann S, Freeman E, Haynes JD, *et al.* (2006): Concurrent TMS-fMRI and psychophysics reveal frontal influences on human retinotopic visual cortex. Curr Biol 16:1479–1488.
113. Hanlon CA, Dowdle LT, Moss H, Canterberry M, George MS (2016): Mobilization of medial and lateral frontal-striatal circuits in cocaine users and controls: An interleaved TMS/BOLD functional connectivity study. Neuropsychopharmacology 41:3032–3041.
114. Chen AC, Oathes DJ, Chang C, Bradley T, Zhou ZW, Williams LM, *et al.* (2013): Causal interactions between fronto-parietal central executive and default-mode networks in humans. Proc Natl Acad Sci U S A 110:19944–19949.
115. Fox MD (2018): Mapping symptoms to brain networks with the human connectome. N Engl J Med 379:2237–2245.